Integrated effective emissivity computation for non-isothermal non-axisymmetric cavities

Dong Liu (刘 东), Yuanyuan Duan (段远源)*, and Zhen Yang (杨 震)

Key Laboratory of Thermal Science and Power Engineering of Ministry of Education,
Beijing Key Laboratory for CO_2 Otilization and Reduction Technology,
Tsinghua University, Beijing 100084, China

**Corresponding author: yyduan@tsinghua.edu.cn*

Received June 4, 2012; accepted August 7, 2012; posted online January 21, 2013

Non-axisymmetric cavities are widely used as standard blackbody sources for radiation thermometry. The integrated effective emissivity is central to the blackbody design. Integrated effective emissivities are numerically calculated for non-isothermal, non-axisymmetric cavities. The average relative deviation is 0.087% when compared with Monte-Carlo results, indicating that this method can accurately calculate the integrated effective emissivities for non-isothermal, non-axisymmetric cavities. The effects of the wavelength, temperature uniformity, and bottom inclination angle are then analyzed.

OCIS codes: 200.0200, 120.0120.
doi: 10.3788/COL201311.022001.

Methods that accurately predict the integrated effective emissivities of blackbody designs are needed. Many computational methods have been developed for axisymmetric cavities such as conical, cylindrical and cylindro-conical[1−8], cylindrical with a re-entrant cone bottom[9], and cylindrical and cylindro-conical cavities with grooved walls[10−12]. Non-axisymmetric cavities are also widely used as standard blackbody sources for radiation thermometry[13−17]. However, very few studies have reported on methods that analyze non-axisymmetric cavities because of the complex computations for configuration factors. Prokhorov *et al*. computed the integrated effective emissivities of isothermal non-axisymmetric cavities for the first time in 2004[18] and of non-isothermal non-axisymmetric cavities in 2010[19] using the Monte Carlo method. Although effective, the Monte Carlo method is time-consuming and lacks validation for the integrated effective emissivity of non-axisymmetric cavities.

Computational methods require verification to ensure computational accuracy because the experimental determination of the integrated effective emissivity is limited to restricted geometries, spectral ranges, and cavity temperatures[18]. Duan *et al*.[20] reported integrated effective emissivity computations for isothermal non-axisymmetric cavities using the finite element method; these results agreed well with those of the Monte Carlo method. However, real cavities are not isothermal. Thus, isothermal approximations are insufficient. Therefore, this letter presents a natural extension of the isothermal non-axisymmetric cavity computations to non-isothermal non-axisymmetric cavities. The computational results are compared with previous Monte Carlo results[19], which are the only known findings for the integrated effective emissivity of non-isothermal, non-axisymmetric cavities.

Figure 1 shows the geometric configuration and temperature distribution of a cavity. The cavity is a cylinder with an inclined bottom. R is the cavity aperture radius, H is the cavity length, $H_{\rm d}$ is the distance from the detector to the cavity aperture, $R_{\rm d}$ is the detector radius, and β is the bottom inclination angle. The inclined bottom extends from $z_{\min}$ to $-z_{\min}$. Dimensionless geometrical parameters were used because of the scaling properties. R was set to 1 for simplicity. The temperature distribution is[19]

$$T(Z)=\begin{cases} T_{\rm b}, & Z_{\min}\leqslant Z\leqslant Z_{\rm b} \\ T_{\rm b}+\dfrac{T_{\rm b}-T_{\rm a}}{Z_{\rm b}-Z_{\max}}(Z-Z_{\rm b}), & Z_{\rm b}\leqslant Z\leqslant Z_{\max} \end{cases}. \tag{1}$$

The material for the entire inner wall of the cavity was assumed to be uniform and grey so that the radiating cavity surfaces were spatially uniform and independent of the wavelength and to ensure that the surfaces exhibit diffused emissions and reflections.

The local directional spectral effective emissivity of a non-isothermal cavity in a non-refractive environment is

$$\varepsilon_{\lambda,{\rm e}}(\lambda,\vec{\xi},\vec{\omega},T_{\rm ref})=\frac{L_\lambda(\lambda,\vec{\omega},\vec{\omega})}{L_{\lambda,{\rm b}}(\lambda,T_{\rm ref})}, \tag{2}$$

where L_λ is the spectral radiance emitted from a point $\vec{\xi}$ with a local temperature $T\big(\vec{\xi}\big)$ on the cavity wall at a particular wavelength λ and in the direction of $\vec{\omega}$; $L_{\lambda,{\rm b}}$ is the spectral radiance of a perfect blackbody at a reference temperature $T_{\rm ref}$ at the same wavelength and direction. The bottom center temperature of the cavity was used as the reference temperature.

The integrated effective emissivity is defined as

$$\varepsilon_{\lambda,{\rm e}}(\lambda,T_{\rm ref},R_{\rm d},H_{\rm d})=\frac{\Phi_\lambda(\lambda,R_{\rm d},H_{\rm d})}{\Phi_{\lambda,{\rm b}}(\lambda,T_{\rm ref},R_{\rm d},H_{\rm d})}, \tag{3}$$

where $\Phi_\lambda(\lambda,R_{\rm d},H_{\rm d})$ is the spectral radiant flux falling onto the black detector that is irradiated by the radiating cavity surfaces, and $\Phi_{\lambda,{\rm b}}(\lambda,T_{\rm ref},R_{\rm d},H_{\rm d})$ is the spectral radiant flux falling onto the same detector that is irradiated by a cavity with perfectly black walls. The integrated effective emissivity can be derived from Eq. (2)

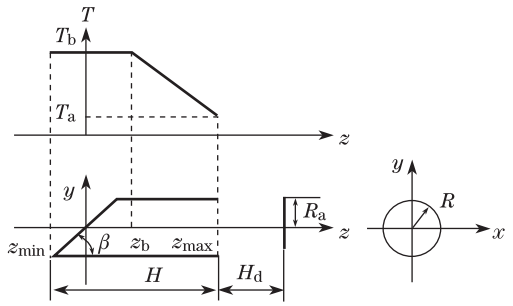

Fig. 1. Cavity geometry and temperature distribution.

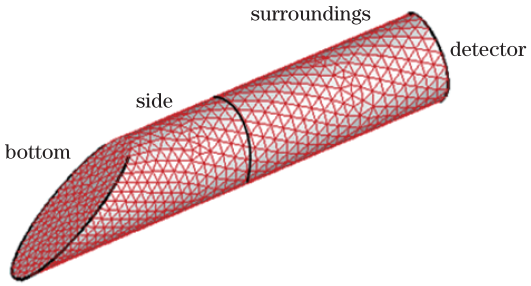

Fig. 2. Computational grid.

via integration over the appropriate areas and solid angles.

The numerical method for non-isothermal cavities is similar to that used in Ref. [20] for isothermal cavities. The outgoing flux from the radiating cavity surface consists of the flux that is intrinsically emitted and that reflected after incidence from the other radiating cavity surfaces. Therefore, the spectral outgoing radiant flux of a radiating cavity surface element is expressed as

$$J_{\lambda,k} = E_{\lambda,k} + (1-\varepsilon_{\lambda,k}) \sum_{j=1}^{N} F_{k,j} J_{\lambda,j}, \tag{4}$$

where $E_{\lambda,k}$ is the spectral radiant flux emitted by a radiating surface element, $\varepsilon_{\lambda,k}$ is the spectral emissivity of the radiating cavity surface, $F_{k,j}$ is the configuration factor for two surface elements, and N is the number of surface elements. The local spectral radiant flux is calculated by iteratively solving Eq. (4). The spectral radiant flux that falls onto the black detector irradiated by the radiating cavity surfaces is

$$\Phi_{\lambda}(\lambda, R_{\rm d}, H_{\rm d}) = \sum_{k=1}^{N} F_{k,{\rm d}} J_{\lambda,k}, \tag{5}$$

where $F_{k,{\rm d}}$ is the configuration factor for one surface element and the detector. The spectral radiant flux falling onto the same detector that is irradiated by the cavity with perfectly black radiating surfaces is given by

$$\Phi_{\lambda,{\rm b}}(\lambda, T_{\rm ref}, R_{\rm d}, H_{\rm d}) = \sum_{k=1}^{N} F_{k,{\rm d}} J_{\lambda,k,{\rm b}}, \tag{6}$$

where $J_{\lambda,k,{\rm b}}$ is the spectral outgoing radiant flux of a perfect black surface element. Thus, the integrated effective emissivity is calculated as

$$\varepsilon_{\lambda,{\rm e}}(\lambda, T_{\rm ref}, R_{\rm d}, H_{\rm d}) = \frac{\Phi_{\lambda}(\lambda, R_{\rm d}, H_{\rm d})}{\Phi_{\lambda,{\rm b}}(\lambda, T_{\rm ref}, R_{\rm d}, H_{\rm d})} = \frac{\sum\limits_{k=1}^{N} F_{k,{\rm d}} J_{\lambda,k}}{\sum\limits_{k=1}^{N} F_{k,{\rm d}} J_{\lambda,k,{\rm b}}}. \tag{7}$$

The configuration factors were calculated using the surface-to-surface model in ANSYS FLUENT according to the geometry and the grid.

Given that the emissivity of a non-isothermal cavity changes with the wavelength, the radiant flux should be calculated using Planck's Law. However, ANSYS FLUENT can only calculate the radiant flux over the entire spectrum using the Boltzmann formula. Therefore, to calculate the radiation transport at a specific wavelength, the radiating cavity surface temperature of an inner wall element in FLUENT was set to an equivalent temperature $T_{\rm e}$. Thus, the most crucial factors such as the geometry and temperature distribution are considered, and the heat flux at this element, as calculated in FLUNET, is equal to the spectral radiant flux calculated using Planck's Law. In this process, the radiation transport at each spectrum can still be modeled using the available FLUENT model. The transformation equation is

$$\sigma T_{\rm e}^4 = \frac{c_1 \lambda^{-5}}{\exp(\frac{c_2}{\lambda T}) - 1} \Rightarrow T_{\rm e} = \sqrt[4]{\frac{c_1 \lambda^{-5}}{\sigma \exp(\frac{c_2}{\lambda T}) - 1}}, \tag{8}$$

where T is the real radiating surface temperature, $T_{\rm e}$ is the transformed radiating surface temperature, $c_1 = 3.74177118(19) \times 10^{-16}$ W·m^2, $c_2 = 1.4387752(25) \times 10^{-2}$ m·K, and $\sigma = 5.670400(40) \times 10^{-8}$ W·m^{-2} K^{-4}. The radiating cavity surface temperature distribution was defined using a UDF.

Figure 2 shows the computational grid. The detector and the surrounding media between the detector and the cavity aperture do not affect the radiative transfer. Therefore, the detector and the surrounding emissivity were set to 1, and the temperature was set to 0 K.

The integrated effective emissivities of non-isothermal axisymmetric cylindrical cavities with various λ and $z_{\rm b}$ were calculated at $R_{\rm d} = 1$, $H = 8$, $H_{\rm d} = 0$, $\varepsilon = 0.7$, $T_{\rm b} = 1\,000$, and $T_{\rm a} = 990$ to validate the developed method. Table 1 shows the computational results for various numbers of elements at $z_{\rm b} = 0$. The average relative difference is 0.034%, indicating that the present number of elements is sufficient to ensure high accuracy for adoption in the calculations. Figure 3 compares the results calculated using the present method and those of the Monte Carlo method. The average relative difference is 0.096%, indicating that the present method is accurate.

Figure 4 shows the results for non-isothermal non-axisymmetric cavities for various λ, $z_{\rm b}$, and β at $R_{\rm d} = 1$, $H = 8$, $H_{\rm d} = 0$, $\varepsilon = 0.7$, $T_{\rm b} = 1\,000$, and $T_{\rm a} = 990$. The results are again compared with the Monte-Carlo results. The average relative difference is 0.087%, which confirms that the present method can effectively predict the

Table 1. Grid Independence

λ (μm)	267823 Elements	829345 Elements	Relative Difference (%)
1	0.813462	0.813168	0.0361
3	0.880196	0.879894	0.0343
5	0.893332	0.893028	0.0340
7	0.898693	0.898389	0.0338
9	0.901408	0.901104	0.0337

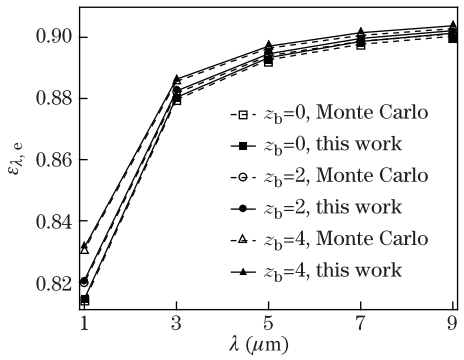

Fig. 3. Method validation.

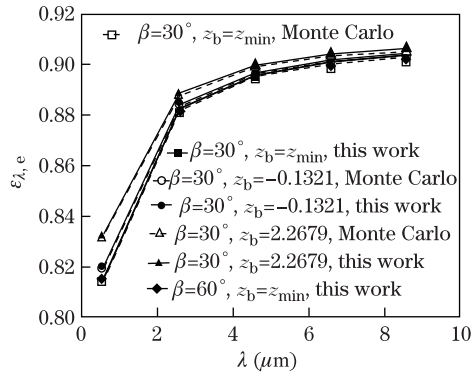

Fig. 4. Computational results.

integrated effective emissivities of non-isothermal, non-axisymmetric cavities. The results also show that the integrated effective emissivity increases with wavelength and temperature uniformities; however, the effect of temperature uniformity decreases at longer wavelengths. The cavity bottom inclination angle has negligible effect on the integrated effective emissivities.

In conclusion, integrated effective emissivities are numerically calculated for non-isothermal, non-axisymmetric cavities. The results are consistent with those of the Monte-Carlo method. The average relative difference between the two results is 0.087%, which indicates that this method can effectively calculate the integrated effective emissivities of non-isothermal, non-axisymmetric cavities. The integrated effective emissivity increases with the wavelength and temperature uniformities. However, the effect of temperature uniformity is negligible at long wavelengths. The cavity bottom inclination angle has little effect on the integrated effective emissivities.

This work was supported by the National "973" Program of China under Grant No. 2009CB219805.

References

1. R. P. Heinisch, E. M. Sparrow, and N. Shamsund, J. Opt. Soc. Am. **63,** 152 (1973).
2. A. Ono, J. Opt. Soc. Am. **70,** 547 (1980).
3. Z. Chu, J. Dai, and R. E. Bedford, *AIP Conf. Proc. Temperature*: *Its Measurement and Control in Science and Industry* 907 (1992).
4. V. I. Sapritsk and A. V. Prokhorov, Metrologia **29,** 9 (1992).
5. M. J. Ballico, Metrologia **32,** 259 (1996).
6. V. I. Sapritsky and A. V. Prokhorov, Appl. Opt. **34,** 5645 (1995).
7. J. Hartmann, D. R. Taubert, and J. Fischer, in *Proceedings of 7th International Symposium on Temperature and Thermal Measurements in Industry and Science* 511 (1999).
8. A. S. Nester and J. R. Mahan, Proc. SPIE **4710,** 9 (2002).
9. H. C. McEvoy, G. Machin, R. Friedrich, J. Hartmann, and J. Hollandt, *AIP Conf. Proc. Temperature*: *Its Measurement and Control in Science and Industry* 909 (2003).
10. J. Ishii, M. Kobayashi, and F. Sakuma, Metrologia **35,** 175 (1998).
11. Y. Te, P. Jeseck, C. Camy-Peyret, S. Payan, S. Briaudeau, and M. Fanjeaux, Metrologia **40,** 24 (2003).
12. H. Zhang and J. Dai, Chin. Opt. Lett. **4,** 306 (2006).
13. U. Mester and P. Winter, Proc. SPIE **4360,** 372 (2001).
14. J. Ishii and A. Ono, Meas. Sci. Technol. **12,** 2103 (2001).
15. J. Ishii, T. Fukuzaki, T. Kojima, and A. Ono, in *Proceedings of 8th International Symposium on Temperature and Thermal Measurements in Industry and Science* 729 (2001).
16. H. McEvoy, R. Simpson, and G. Machin, Proc. SPIE **5405,** 54 (2004).
17. A. Diril, H. Nasibov, and S. Ugur, *AIP Conf. Proc. Temperature*: *Its Measurement and Control in Science and Industry* 663 (2003).
18. A. V. Prokhorov and L. M. Hanssen, Metrologia **41,** 421 (2004).
19. A. V. Prokhorov and L. M. Hanssen, Metrologia **47,** 33 (2010).
20. Y. Duan, D. Liu, J. Wang, and Z. Yang, J. Therm. Sci. Technol. **11,** 125 (2012).